JGR Atmospheres

RESEARCH ARTICLE
10.1029/2024JD041860

The Hawaii Dust Regime: Patterns and Variability in Aerosol Mineral Dust From MERRA-2 at Station ALOHA and the Hawaii Aerosol Time-Series

Daniel C. Ohnemus[1], Charlotte Kollman[1], Christopher M. Marsay[1,2], Mariah Ricci[1], and Clifton S. Buck[1]

[1]University of Georgia, Department of Marine Sciences, Skidaway Institute of Oceanography, Savannah, GA, USA, [2]Now at: University of Delaware, School of Marine Science and Policy, College of Earth, Ocean and Environment, Newark, DE, USA

Abstract The transport and delivery of low-abundance, bioactive trace elements to the surface ocean by aerosol mineral dust is a major planetary control over marine primary production and hence the global carbon cycle. Variations in the concentration of atmospheric dust have established links to global climate over geologic timescales and to regional biogeographic shifts over seasonal timescales. Constraining atmospheric dust variability is thus of high value to understanding oceanographic systems, especially vast, constitutively low-nutrient subtropical gyre ecosystems and high-nutrient/low-chlorophyll ecosystems where availability of the trace element iron is a dominant ecological control. Here we leverage the MERRA-2 reanalysis product to examine over four decades of surface-level atmospheric mineral dust concentrations in a domain of the subtropical North Pacific centered at Ocean Station ALOHA. This study region has been sampled regularly since the mid-1980s and was the site of the Hawaii Aerosol Time-Series (HATS) project in 2022–2023. Two unequal semi-annual periods of elevated dust evident in the long-term results are described and constrained. We look for evidence of shifts in total and seasonal atmospheric dust abundances or in the timing of the onset of the dominant spring/summer dusty period, finding year-to-year variations but little evidence for long-term trends. We observe significant but complex relationships between the Pacific Decadal Oscillation (PDO) index and both dust and precipitation. The 2022 calendar year was among the dustiest years for the study domain in the preceding two decades and, by contrast, 2023 exhibited a significant early spring lull in dust.

Plain Language Summary Dust blown from Earth's continents fertilizes the oceans with iron and other nutrients needed for plants to grow. This affects ocean ecosystems and is an important control on Earth's climate. Modern models for the atmosphere report dust very precisely in time and space but rarely address how it affects specific ocean sites over time. We examine these best-available model outputs for a well-studied site at Hawaii to improve our understanding of how dust has varied over the many decades this region has been studied by oceanographic and atmospheric researchers.

Key Points:

- Mineral dust concentrations from the MERRA-2 atmospheric reanalysis product are investigated at Hawaii's ocean Station ALOHA back to 1980
- Two semi-annual dust pulses at the site are described and little evidence is seen for long-term shifts in total dust or pulse timing
- Dust concentrations exhibit different periodicities and relationships with precipitation and Pacific Decadal Oscillation index

Supporting Information:

Supporting Information may be found in the online version of this article.

Correspondence to:

D. C. Ohnemus,
dan@uga.edu

Citation:

Ohnemus, D. C., Kollman, C., Marsay, C. M., Ricci, M., & Buck, C. S. (2025). The Hawaii dust regime: Patterns and variability in aerosol mineral dust from MERRA-2 at station ALOHA and the Hawaii aerosol time-series. *Journal of Geophysical Research: Atmospheres*, *130*, e2024JD041860. https://doi.org/10.1029/2024JD041860

Received 24 JUN 2024
Accepted 14 DEC 2024
Corrected 18 JAN 2025

This article was corrected on 18 JAN 2025. See the end of the full text for details.

Author Contributions:

Conceptualization: Daniel C. Ohnemus
Data curation: Daniel C. Ohnemus
Formal analysis: Daniel C. Ohnemus
Funding acquisition: Daniel C. Ohnemus, Christopher M. Marsay, Clifton S. Buck
Investigation: Daniel C. Ohnemus, Charlotte Kollman, Christopher M. Marsay, Mariah Ricci, Clifton S. Buck
Methodology: Daniel C. Ohnemus

1. Introduction

Aerosol mineral dust blown from continental sources and deposited into the upper ocean is a major source of low-abundance trace elements to seawater (Jickells et al., 2016). The supply of dust-sourced trace elements—most notably iron, but also manganese, copper, zinc, and others—exerts global-scale effects on marine biogeography and the extent of marine primary production (Browning & Moore, 2023; Jickells & Moore, 2015). Dust-derived lithogenic particles are also a key component of the ocean's vertical particle flux thereby affecting the internal cycling of carbon, macronutrients, and micronutrient elements (Bressac et al., 2014, 2019; Conte et al., 2019; Honjo, 1982; Huang & Conte, 2009; Lamborg et al., 2008).

Despite the critical importance of dust to many global biogeochemical processes—including biological carbon and nitrogen fixation and the biological carbon pump—it remains an ephemeral and difficult-to-constrain oceanic input (Anderson et al., 2016; Wu et al., 2020). Atmospheric concentrations of dust are highly variable in time and space because of the episodic nature of dust mobilization at the source driven by local meteorological conditions as well as larger-scale variations in downwind atmospheric transport. Dust inputs furthermore originate from multiple land source regions which are known to exert proportionally different levels of influence at different times of year. For example, Asian dust, including that from the Middle East and central Asian sources, contributes

Project administration: Clifton S. Buck
Resources: Daniel C. Ohnemus
Software: Daniel C. Ohnemus
Supervision: Daniel C. Ohnemus, Clifton S. Buck
Validation: Daniel C. Ohnemus
Visualization: Daniel C. Ohnemus
Writing – original draft: Daniel C. Ohnemus, Charlotte Kollman, Christopher M. Marsay, Mariah Ricci, Clifton S. Buck
Writing – review & editing: Daniel C. Ohnemus, Charlotte Kollman, Christopher M. Marsay, Mariah Ricci, Clifton S. Buck

approximately 40% to global dust loading and has outsized influence throughout most of the North Pacific basin, but its relative contribution can vary between 100% and 0% depending on the exact oceanographic site and time of year (Kok et al., 2021). For the critical bio-active element iron, significant variations in the relative loading of anthropogenic and pyrogenic aerosols can shift widely on both event-level and interannual timescales, further complicating aerosol temporal variability and oceanographic impacts (Hamilton, 2020; Schroth, 2009; Weis, 2022).

The Hawaii Aerosol Time-Series (HATS) was a 2-year field project focused on constraining aerosol dust composition, mineralogy, and chemical lability; measuring dry and wet dust deposition fluxes; and tracking dust's post-depositional fate in the upper ocean. The HATS field campaign concluded in December 2023 and combined continuous, weeklong integrated sampling of surface-level bulk aerosols and rain on the windward (eastern) side of the island of Oahu with six oceanographic expeditions to Station ALOHA in association with the Hawaii Ocean Time-series (HOT) program (Bates et al., 2014; Karl et al., 1996; Karl & Lukas, 1996). Station ALOHA is located c.a. 100 km north of Oahu in the oligotrophic waters of the North Pacific subtropical gyre. Previous observations and modeling work show that dust transported to the Hawaii region predominantly originates from source regions in the Middle East and Central and Eastern Asia with additional contributions from the North American southwest and Africa (Huneeus et al., 2011; Jickells et al., 2016; Kok et al., 2021; Mahowald et al., 2005). The HATS project used the cosmogenic nuclide beryllium-7 (^{7}Be) as a tracer for bulk deposition, which includes both wet and dry deposition processes, to provide estimates of dust flux to the surface ocean during the study (Kadko et al., 2015). We analyzed collected aerosols for chemical composition and trace element lability with a multi-element approach inspired by the U.S. CLIVAR (now GO-SHIP) and international GEOTRACES programs (Buck et al., 2013, 2019; Marsay et al., 2022), to monitor chemical variability in dust transported to the region during calendar years 2022 and 2023.

The oceanographic impacts of dust deposition are a function of the flux rate and other factors including the fractional solubility of bioactive trace elements. Flux is a function of both dust concentration and deposition velocity, a variable term itself impacted by several factors, and is inherently challenging to measure due to both the intermittence of dusty periods and limited access to remote oceanographic sites (Kadko et al., 2015; Schulz et al., 2012). In lieu of directly capturing flux rates, the research community applies various means to estimate flux (e.g., Duce et al., 1991; Kadko et al., 2020) and all methods, including those applied to MERRA-2 products, introduce uncertainties by way of their calculation. Atmospheric dust concentrations, however, can be estimated with high spatiotemporal coverage via satellite-derived aerosol optical depth. Concentrations are generally better-resolved and ground-truthed in atmospheric models than deposition (Hunneus et al., 2011; Wu et al., 2020), despite the latter exerting more direct forcing on oceanographic systems. Given the importance of dust concentrations to both dry and wet deposition rates, and to better inform our forthcoming comprehensive field results from HATS where deposition and other oceanographic implications will be explicitly examined, we focus here on constraining atmospheric dust concentrations near Hawaii and examining their variability from day-to-day (hereafter, "events"), across seasons (hereafter seasonal dust "pulses"), and from year-to-year (inter-annual variations).

The relevance of both short- and long-timescale forcings of dust are indicated by many observations of marine trace element behaviors. Previous studies have applied a range of techniques to estimate residence times for dust and dust-derived elements in the euphotic upper ocean, particularly the best-studied dust-derived element iron, and have found these to be on the order of days to months (Black et al., 2019, 2020; Fitzsimmons et al., 2015; Hawco et al., 2022; Hayes et al., 2015; Ohnemus & Lam, 2015; Tagliabue et al., 2023). As a result of these short residence times, oceanographic studies of trace elements typically focus only on local and contemporaneous dust data when contextualizing upper ocean field results (Boyle et al., 2005; Fitzsimmons et al., 2015; Hayes et al., 2015; Rijkenberg et al., 2008; Winton et al., 2014). Atmospheric studies, by comparison, typically examine multiple atmospheric components over very large spatial scales with the aim of summarizing dust transport and delivery over basin-wide swaths (Huneeus et al., 2011; Kok et al., 2021).

There is a notable literature gap, both spatially and temporally, examining dust delivery patterns on seasonal and interannual scales in regional proximity to major oceanographic sites like Station ALOHA. This gap results in missing context that hinders interpretation of data sets emerging from repeated sampling campaigns like HATS and potentially longer-running time-series programs like HOT. In the region around Hawaii specifically, many oceanographic studies utilize a single long-term atmospheric monitoring site at Mauna Loa Observatory

(MLO)—which samples the free troposphere at an altitude of 3,397 m—to provide atmospheric dust context for sea-level observations in the planetary boundary layer. Sampling records from MLO continue to have high oceanographic value due to their inclusion of elemental data for Fe and other lithogenic tracer elements like Al and Ti for a period from 1988 to early 2011 (Hyslop et al., 2013). While ongoing MLO sensor data are continuous, the MLO elemental records are nevertheless intermittent—having sampled only during specific days of the week and at certain times of day—and are likely to have missed important shorter-scale dust events. One may reasonably question the degree to which aerosol loading, particle size distribution, and chemical lability measured at MLO are comparable for dust at the ocean's surface.

To address these gaps, this study investigates and parameterizes the dust regime around the Hawaiian Islands on daily to decadal bases using the Modern-Era Retrospective Analysis for Research and Applications, Version 2 (MERRA-2) reanalysis product as a data source (Buchard et al., 2017; Gelaro et al., 2017; Randles et al., 2017). Focusing on the planetary boundary layer where the ocean and atmosphere interact, we address several questions aimed at providing context for dust-related processes in this important oceanographic system, with a particular focus on dust concentration variability. How do dust concentrations in the lower atmosphere typically vary on day-of-year and year-over-year bases, and what is the variability throughout the year? How significant and variable are different multi-month seasonal dust pulses vis-a-vis their extent, timing, and overall contributions to annual dust loading? Which years in the record were comparatively high or low dust, and what are typical lengths of individual dust events in the region? How significant are the product's dust correlations with precipitation and the Pacific Decadal Oscillation (PDO) climatological index, identified as an important control in earlier work (Letelier et al., 2019)? Finally, we place the HATS program field sampling years of 2022 and 2023 within the context of the available record.

2. Methods

2.1. Data Sources and Availability

The MERRA-2 collection—specifically V5.12.4, M2T1NXAER: hourly, time-averaged 2-D aerosol diagnostics—was spatially subset for the study domain described below and downloaded via the NASA Goddard Earth Sciences Data and Information Services Center (GMAO, 2015). This version and subset of the product consists of hourly, time-averaged, assimilated aerosol diagnostics including the concentration of aerosol components black carbon, dust, sea salt, sulfate, and organic carbon. For a subset of precipitation comparisons, we examine the *PRECTOTCORR* corrected precipitation totals from the M2T1NXAER collection. In this study, we utilized product outputs from 1980-Jan-01 through 2023-Dec-31 unless otherwise noted. Code (MATLAB) used to conduct our analyses and generate the figures can easily be adapted to other spatial subsets of MERRA-2 and are available at the lead author's GitHub page: github.com/capecodnative/HawaiiDust also archived at Zenodo (Ohnemus, 2024).

2.2. Study Region

The study region investigated here (hereafter the "whole domain") is located between 15 ºN, 165 ºW and 28 ºN, 150 ºW (Figure 1), centered on the major Hawaiian Islands.

Station ALOHA is located near the center of the domain at 22.75 ºN, 158 ºW and has been sampled regularly since 1978 by the HOT program and its participants (Karl & Lukas, 1996). MERRA-2 product outputs are grid-centered at the red points shown in Figure 1 which are spaced at 0.5° of latitude and 0.625° of longitude, yielding 675 (25 × 27) datapoints. A sub-domain, shown in blue in the figure and centered at Station ALOHA, is used for a small portion of precipitation analyses. Precipitation is more spatially variable throughout the whole domain than is dust, and the narrower precipitation sub-domain better captures precipitation variations likely to affect the HATS and ALOHA study sites.

2.3. Parameters and Calculations

This study primarily examines variability in the MERRA-2 *DUSMASS* parameter which represents the concentration of mineral dust in kg/m^3 present in the planetary boundary layer, the lowest layer of the atmosphere in the MERRA-2 product. In text and figures, we occasionally reference units of $\mu g/m^3$ for simplicity. While newer derived products (e.g., Kok et al., 2021) have, for instance, used a range of methodologies to improve reanalysis

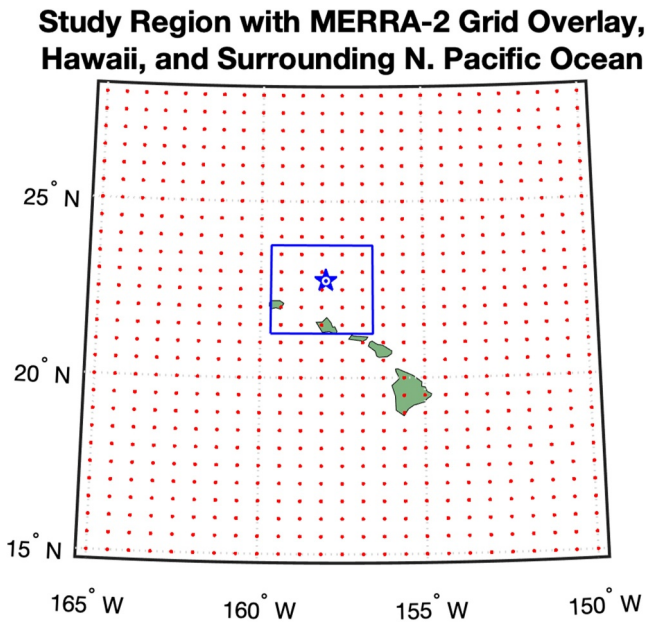

Figure 1. Map of the study region whole domain (black outer box) showing MERRA-2 grid-centered datapoints (red points). There are 675 (25 × 27) points in the domain examined. A sub-domain, outlined in blue and centered at ocean Station ALOHA (blue star and white circle), is used for a subset of precipitation analyses.

products—e.g. better source region apportionment and addressing assumptions of spherical dust shape inherent in MERRA-2—the MERRA-2 product remains among the best available to examine short-to-long term trends in dust concentrations. The MERRA-2 product has good to strong correlation with long-term records of Northern Hemisphere surface dust concentrations and exhibits minimal biases against other atmospheric parameters (Buchard et al., 2017; Gelaro et al., 2017; Randles et al., 2017). The remoteness of our study site places it many thousands of kilometers from major sources of biomass burning and anthropogenic emissions located in Asia and the Americas which can act as sources of interference to reanalysis product estimations.

The whole domain examined here is chosen to be applicable to oceanographic studies located in the Hawaii region, including HATS, HOT, and other studies occupying Station ALOHA or the surrounding waters of the North Pacific. The high temporal resolution (hourly) of the MERRA-2 product was reduced to a daily median value for each grid point. We then calculated a daily grand median across all grid points in the domain. Cumulative dust concentrations, where discussed, were calculated by summing the daily grand median concentrations for the domain across the time periods examined—typically semi-annual or annual. Given the size of the domain (~1440 km N/S; 1475–1613 km E/W), dust concentrations are not likely to be completely independent from day-to-day: for example, a synoptic-scale dust event may enter the domain via its north-eastern quadrant on day 1 and leave the south-western quadrant on day 4. We therefore focus our examination of cumulative dust trends to temporal scales on the semi-annual to annual levels. Comparison of median and mean values as measures of center (calculated within the smaller sub-domain for dust) are nearly identical to the grand median trends calculated and used here for the whole domain. Use of the whole domain and medians as a measure of center, respectively, provide wider spatial coverage and reduce the potential influences of local Hawaiian aerosol sources and event-level noise. This study does not examine the modeled dust deposition estimates available in MERRA-2, as these values likely have greater uncertainties due to their reduced ground-truthing compared to the product's atmospheric dust concentrations.

To examine time-series periodicity and coherence relationships between climatological indicies and the MERRA-2 dust and precipitation estimates, we first calculated surface dust concentration anomalies (for the whole domain) and daily precipitation anomalies (from the ALOHA subdomain, Figure 1). Detrended dust anomalies were calculated by subtracting the ±5-day mean-smoothed daily median dust concentration at each day of the year; similarly, precipitation anomalies were calculated by subtracting the ±15 days mean-smoothed daily mean precipitation at each day of the year. Detrended dust and precipitation anomalies and their unsmoothed raw values were examined alongside the PDO index and NINO4 index accessed via the National Oceanic and Atmospheric Administration's National Centers for Environmental Information (PDO, 2024). Wavelet analyses and wavelet coherence among the time-series was conducted in MATLAB (Mathworks, 2023), using a sampling interval of 1 year/365.25 days for the daily data sets and 1 year/12 months for the monthly climatological indicators.

3. Results

Median daily mineral dust present at the study site (Figures 2 and 3; Table 1) shows two persistent, nearly semi-annual (hereafter "seasonal") pulses roughly corresponding to spring/summer and fall/winter months. The spring/summer pulse ramps up in mid-to-late February, statistically peaks on April 21/22, and declines from mid-May through August. The fall/winter dust pulse (Figure 3, inset)—is generally broader, less intense, and exhibits greater daily relative variability. The fall/winter pulse begins around late August to mid-September, statistically peaks on November 15, and declines rapidly through December until the yearly dust minimum on December 25/26.

Variability about the day-of-year median trend, expressed as relative standard deviations (RSDs; Figure 2, lower panel), is greatest during the decline of the fall/winter pulse in December and January when dust approaches the

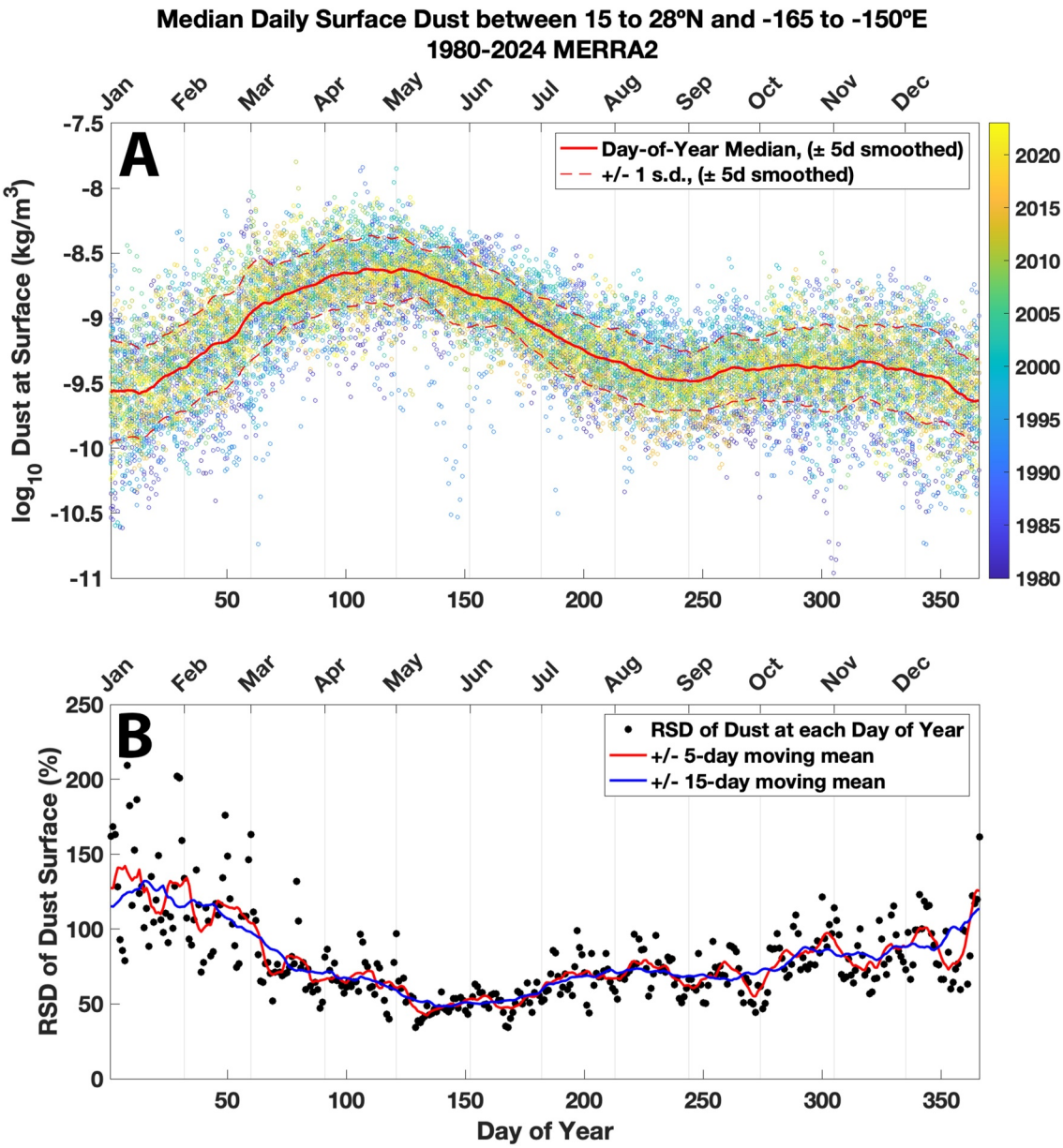

Figure 2. (a) **Upper panel**: Median surface-level atmospheric mineral dust in the whole domain, on a $\log_{10}$ scale (y-axis, $\log_{10}$ kg/m^3) at each day of the year (x-axis, shared both panels). Median trendline for the whole data set and ±1 s.d. lines (all smoothed using ±5 days moving means) are overlaid in red and red-dashed lines, respectively. Datapoint color: year. (b) **Lower panel**: Median-relative standard deviation (RSD) of dust concentrations at each day of the year (black points), which roughly corresponds to the vertical spread between the red dashed lines in the upper panel. Moving means of the daily RSDs are smoothed at ±5 and ±15 days (red and blue lines, respectively) to show trends.

annual minimum. Daily variability is at its minimum during the declining phase of the spring/summer pulse in May and June just following the annual dust maximum in mid-April. Major data set percentiles, dates of the trendline maximum and minimum, and indicators of spread are provided in Table 1. Atmospheric dust concentration extremes range across a factor of ∼1450—between 0.011 and 16 μg dust/m^3. Measures of center, however, including the interquartile range (IQR, 1.0 μg/m^3), ratio of the 75th/25th percentiles (factor of 4.14), and ratio of the 99th/1st percentiles (factor of 22.5) indicate considerably less variability for the majority of days of the year.

Plots of individual years in the record (Figure 4) exhibit the day-to-day fluctuations of dust being transported to and through the study domain. Most individual dust events in the domain exhibit maxima of one to 3 days that

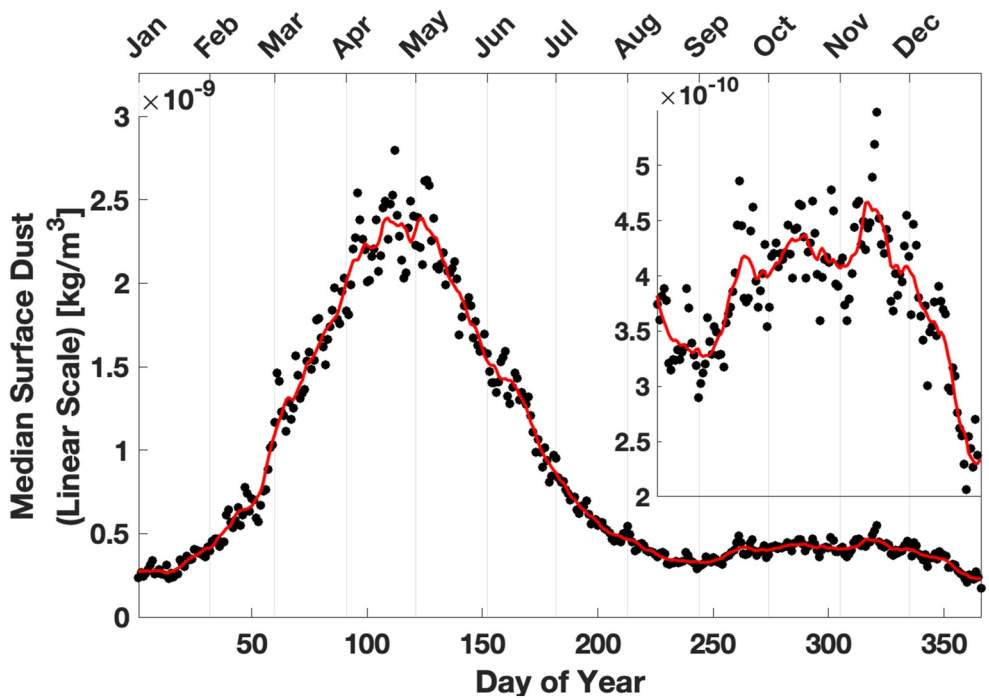

Figure 3. Median dust concentrations (10^{-9} kg/m^3) at each day of the year (black points) on a linear scale, with ±5 days moving mean trendline (red). The spring/summer seasonal dust pulse peaks on April 21/22 and the fall/winter seasonal pulse peaks on Nov 15/16. **Inset**: *y*-axis zoom of the fall/winter seasonal pulse.

build and subside over an additional several days, or up to approximately 2 weeks for longer events. All years, including those shown in Figure 4—the dustiest year on record, 1996; and a more typical year, 2017—exhibit similar patterns of daily to-weekly individual events superimposed on the multi-year trend. Plots of all years in the data set are provided in supplementary materials (Figures S1-1980 to S1-2023 in Supporting Information S1).

The annual dust totals and the cumulative seasonal pulses, split into equal-length half-years (Feb-Jul; Aug-Jan, inclusive), are compared across years in Table 2 and Figure 5. The spring/summer dust pulse accounts for an average of 77.6% of annual dust transport to the site, primarily in March–May, and the fall/winter pulse delivers the remaining 22.4% more evenly throughout the latter half of the year. Four anomalously low-dust years are

Table 1
(a) Dates and Associated Dust Concentrations of the Extremes of the ±5 Day-Smoothed Multiyear Trendline in Figures 2 and 3, (b) Dust Concentrations Associated With Key Percentiles of the Data Set, (c) Ratios of Dust Concentrations at Key Percentiles Indicating Spread for Data Set Extremes and Various Measures of Center

(a) Median trendline	Date	Dust conc. (μg/m^3)
Max Dust	April 20/21	2.80
Min Dust	Dec 25/26	0.207

	(b) Percentiles of daily dust data set, 1980-2023								
	Min. (0%)	1%	5%	25%	50%	75%	95%	99%	Max. (100%)
Surf. Dust (μg/m^3)	0.0110	0.0657	0.138	0.326	0.613	1.35	3.11	4.94	16.0

(c) Ratios of key percentiles	Ratio
Max/Min (100/0%)	1454
99/1%	75.2
95/5%	22.5
75/25%	4.14

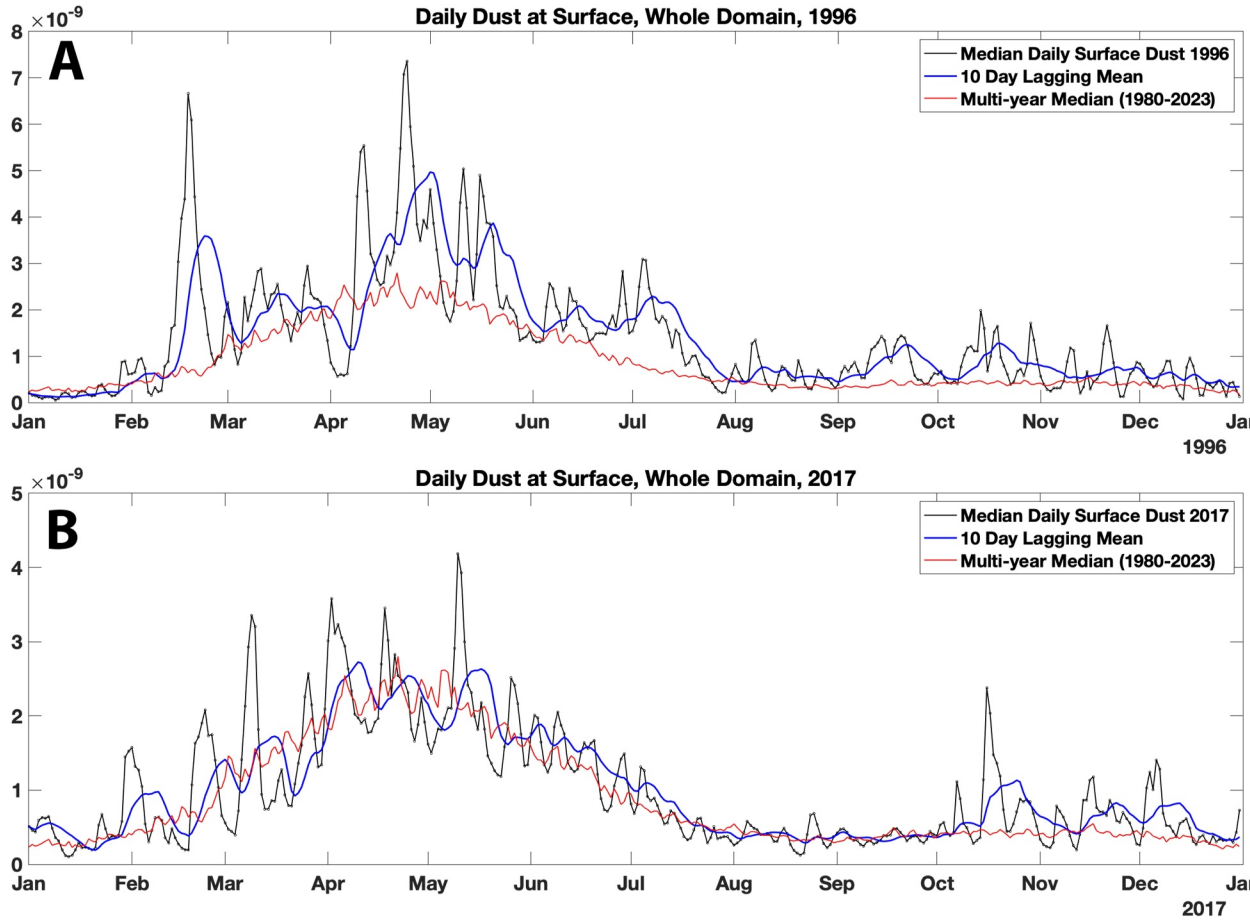

Figure 4. Examples of two individual years of dust over the site highlighting the variability associated with multi-day dust events (individual 'spikes') against the longer-term interannual trends. (a) **Upper panel**: The dustiest year in the record (1996; top) and (b) **Lower panel**: a more typical year (2017; bottom) are shown. Daily data points are in black, 10-day lagging means for each year are in blue, and the multi-year day-of-year median trendline is in red (unsmoothed). Full data plots for all years are available in supplemental materials.

associated with strong atmospheric sulfate injection from large volcanic eruptions that reduced satellite visibility of dust and other atmospheric components in the MERRA-2 product (1982–1983, El Chichón; 1992–1993, Pinatubo). Even excluding these years, no long-term (linear) trends in absolute dust concentrations over the site are apparent: neither total annual dust nor the intensities of either seasonal pulse exhibit significant long-term correlation against year (maximum $R^2 = 0.057$; $p = 0.137$ for annual total dust; supplemental Figure S2 in Supporting Information S1). We used continuous wavelet transformation and coherence analyses to characterize and compare the available dust record to other relevant time-series (Figure 6). The Pacific Decadal Oscillation (PDO) has been previously reported to be a significant predictor of dust delivery to the Hawaii region and the wider eastern N. Pacific subtropical gyre, with positive PDO phases associated with increased dust delivery due to a strengthening of the Aleutian Low (Letelier et al., 2019). Together with a shoaling of the ocean mixed layer and increased upper water column stratification, this set of forcings is proposed to cause a shift in regional ecosystems

Table 2
Cumulative Annual and Seasonal Dust Concentrations (Median ± 1 s.d.), RSDs, and the Percentage of Annual Dust Present in Each Half-Year Period

Annual and seasonal dust	Annual	Spring (Feb–July)	Fall (Aug–Jan)
Cumulative Dust over Domain ±1 s.d. (μg/m^3)	370 ± 66.7	287 ± 56.6	82.8 ± 17.0
RSD (%)	18.0%	19.7%	20.5%
Percentage of Annual Dust Present In Period	100%	77.6%	22.4%

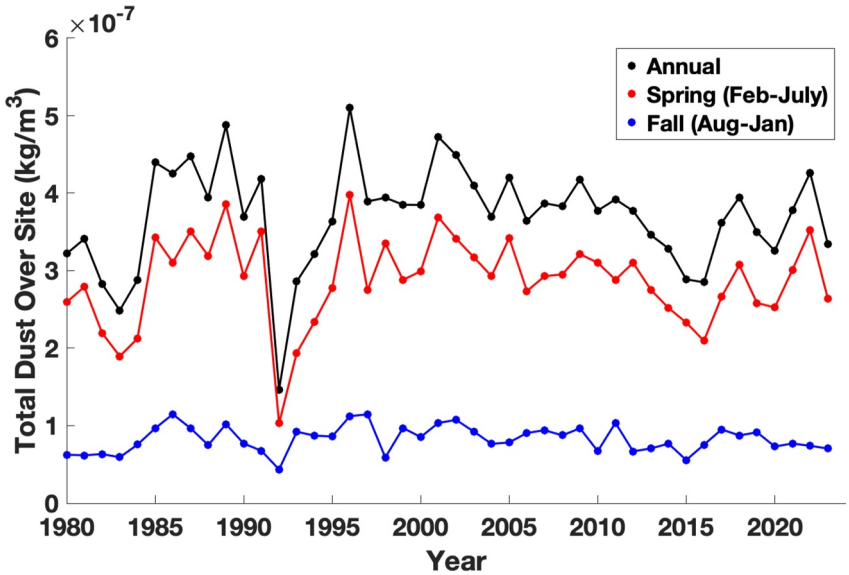

Figure 5. Time-series of total annual cumulative dust concentrations in the study domain (black), along with spring/summer pulse (red), and fall/winter dust pulse (blue) cumulative concentrations. Especially low values in 1982–1983 and 1992–1993 are a data product artifact following atmospheric sulfate injection from major volcanic eruptions (El Chichón and Pinatubo, respectively) which reduced product-derived estimates of all aerosol components including dust. Volcanic-influenced years are excluded from most regression analyses.

from iron-limitation to macronutrient (phosphorus) limitation. We also compare the dust concentration record to precipitation for the Station ALOHA sub-domain, an important connection to deposition. Plots for annually detrended dust anomaly and precipitation anomaly time-series are reported in Figure S3 in Supporting Information S1 and are similar except with reduced power at the 1-year period.

Wavelet analysis of the dust concentration (Figure 6a) and dust concentration anomaly (Figure S3 in Supporting Information S1) time-series clearly show the strong annual and semi-annual periodicity described above. Comparatively minimal periodicity is observed for dust on periods greater than 1 year. Precipitation (Figure 6b) shows a singular, strong annual cycle—but in contrast to dust, no half-year cyclicity—reflecting its characteristically broad but single annual maximum throughout N. Hemisphere winter (see also Figure S4 in Supporting Information S1). The PDO index (Figure 6c), as a decadal-scale climatological indicator, shows its strongest periodic power at multi-year timescales (2-, 5- and 10-year), somewhat irregularly throughout the last 44 years.

We also examined coherence and lag between the dust and precipitation time-series and the PDO index (Figure 6, right column). Comparing dust and precipitation directly (Figure 6e), we observe consistent coherence in their annual cycles (1 year period), along with a fairly consistent lag of dust by one-quarter cycle to slightly more (3–4 months; upward pointing arrows). These results are consistent with the typical seasonality of the individual time-series: a strong spring peak in dust (March/April/May) that lags precipitation's broader maximum from late-fall to early spring (Nov-Mar); see also Figure S3 in Supporting Information S1. Coherence between the PDO index and precipitation (Figure 6f) is stronger and more consistent over the time-series than between PDO and dust (Figure 6d). Precipitation and PDO are most coherent at 2- to 3-year periods, likely reflecting precipitation's more significant multi-year periodicity compared to dust. Lag analysis shows precipitation and PDO are anti-correlated on these multi-year periodicities (left-pointing arrows, Figure 6f) with multi-year minima in precipitation slightly lagging the PDO maxima.

4. Discussion

4.1. Seasonal Dust Pulses and Long-Term Trends in Dust Concentrations

This examination of MERRA-2 mineral dust concentrations over an oceanographically well-studied swath of the Pacific Ocean centered at Hawaii reveals two consistent multi-month seasonal dust pulses (Figures 1–3; Tables 1 and 2). The spring/summer dust pulse spans from approximately February into August, peaks at mid-April, and

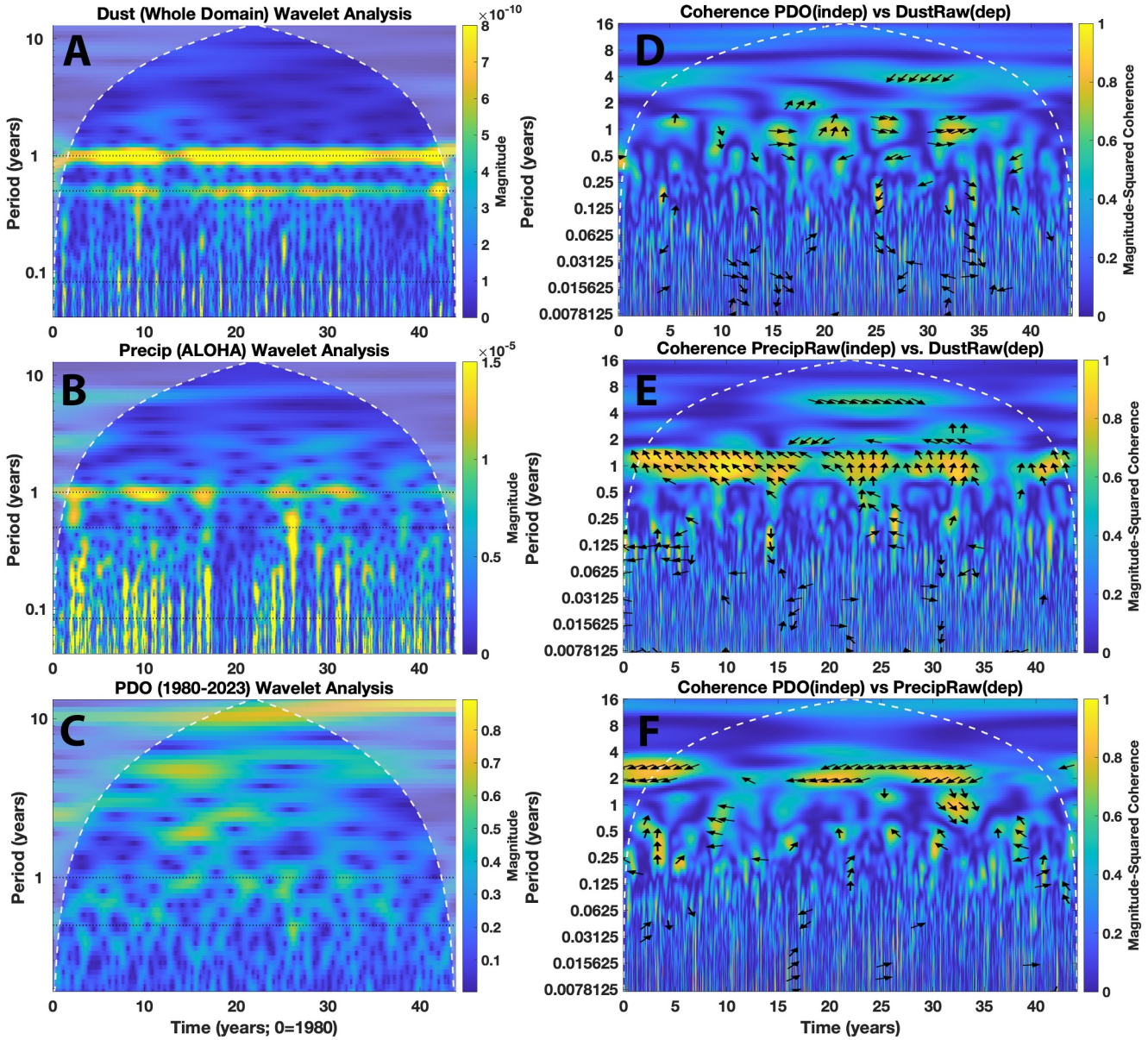

Figure 6. Continuous wavelet transformation (left column) and wavelet coherence diagrams (right column) for the time-series. Individual transforms (left) show the magnitude of periodic signals within each time-series: (a) dust (whole domain); (b) precipitation (ALOHA sub-domain); (c) the PDO index. Dotted horizontal lines are plotted at 1 year, ½ year, and 1 month (when shown) for visual reference. Wavelet coherence diagrams (right column) show the magnitude of frequency overlap between two time-series (independent variable listed first): (d) PDO versus dust; (e) precipitation versus dust; (f) PDO versus precipitation. Where magnitude-squared coherence is > 0.5, time-series lag is indicated by arrows on the unit circle: horizontal-right, in-phase/correlated (no lag); vertical up, y-lagging by ¼ cycle; horizontal-left, out-of-phase/anti-correlated (y-lagging by ½ cycle); vertical down, y-leading by ¼ cycle. Region above the dashed lines (i.e., cone of influence) indicates data set edge effects may be significant.

delivers approximately 78% of the annual dust concentrations over the site. The fall/winter dust pulse spans from September through January, peaks in mid-November, and delivers the remaining 22% of dust. Atmospheric dust concentrations across the 44-year data set span three orders of magnitude, but the variability in dust abundances for most days of the year is considerably more moderate: median daily deviations from the interannual trend are typically only between 50% and 200%. Individual dust events in the region typically span several days or weeks with event-level maxima typically lasting one to 3 days.

We find that the absolute amount of dust being delivered to the study region has not significantly changed since 1980 (Figure 5), nor has the magnitude of the seasonal or semi-annual pulses (Figure S2 in Supporting

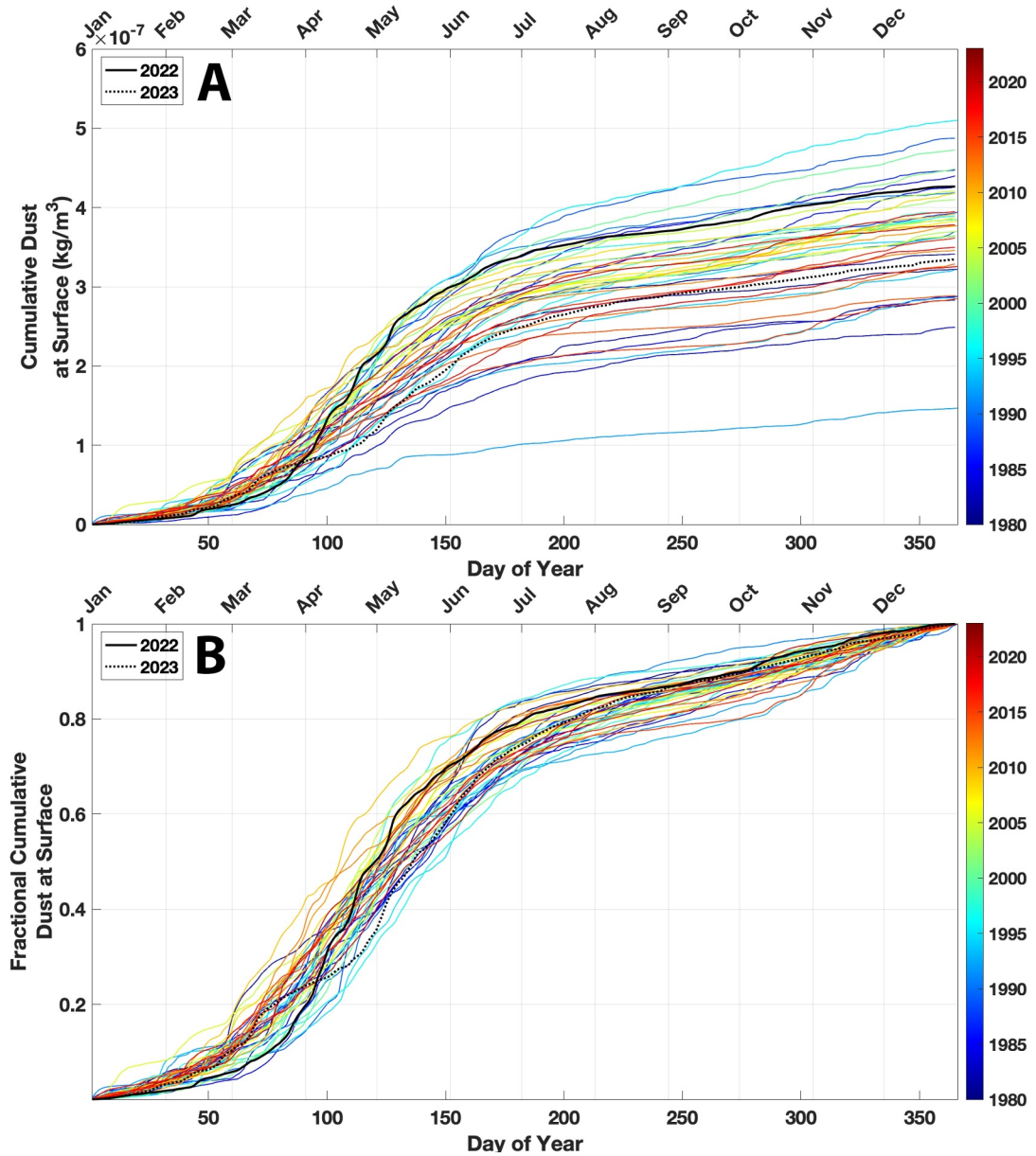

Figure 7. (a) **Upper panel**: Cumulative dust and (b) **Lower panel**, fractional annual cumulative dust (lower panel) present in the study domain for each year of the data set (individual lines, colors). Text labels in the upper panel identify the dustiest 3 years. Two very low-dust years—a data product artifact following major volcanic eruptions—are indicated. In both panels, the HATS program field sampling years of 2022 and 2023 are highlighted in black and black-dashed lines, respectively.

Information S1), though slopes through both annual and seasonal data are all broadly negative. The existence of two discernible dust signals in the data, each evident over long periods of time (Figure 6), behooves their independent consideration. Forthcoming field results from HATS will examine these pulses' intrinsic aspects—e.g. fractional solubility, seasonal shifts in anthropogenic loading, mineralogical composition, and potential for local versus distal sourcing—as well as their extrinsic interactions with relevant atmospheric and oceanographic parameters (e.g., deposition velocities and fluxes and ocean residence times for major bioactive elements).

4.2. Spring Pulse Onset Timing and Dominance; Relevance of the Winter Pulse

The intense spring dust pulse dominates visualizations of both absolute and fractional cumulative dust curves for all years in the record (Figure 7). Fractional cumulative dust is defined as the portion of annual dust observed to

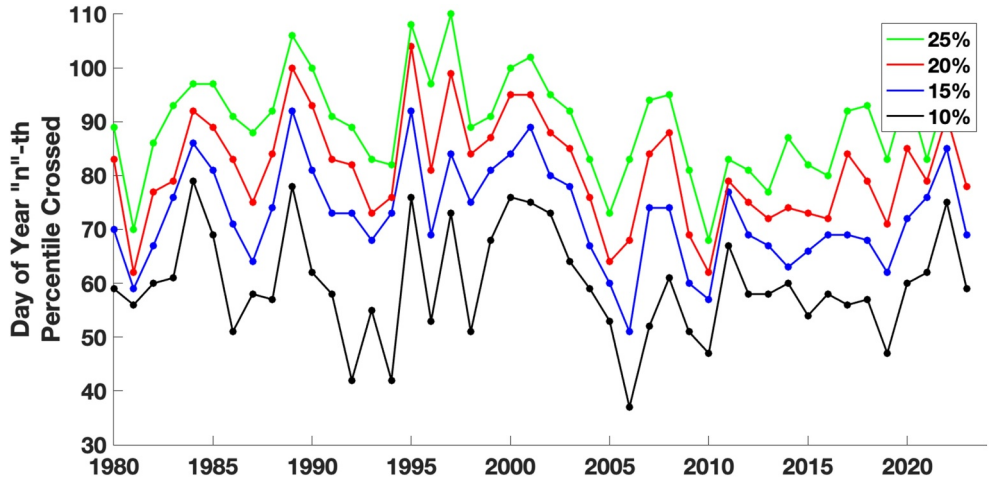

Figure 8. The onset date of the spring pulse as indicated by the day of year (*y*-axis) that the "n"-th percentile of total fractional annual dust was crossed. A range of threshold percentiles for "n" between 10% and 25% are shown, chosen to screen for the onset of the spring/summer dust pulse.

date at each day of the year between January 1 and December 31. Our analysis finds an approximately 2.5-fold spread in the total amount of dust over the region from year to year, excluding years where MERRA-2 product estimates are impacted by vulcanism. The fall/winter pulse is smaller by comparison, but also exhibits higher relative daily variability (Figure 2) and, importantly, delivers dust during the months when surface ocean Chlorophyll-α is at its mixing-driven maximum as observed via satellite and long-term sampling records from Station ALOHA (Karl et al., 1996).

Both dust pulses are thus relevant to understanding trace element dynamics at the ALOHA site, especially given that surface ocean residence times of iron range from weeks to months (Fitzsimmons et al., 2015; Hayes et al., 2015) with those for refractory dust mineral particles potentially being even shorter (Conte et al., 2019; Ohnemus & Lam, 2015). We also note that the two seasonal pulse intensities are not fully independent—their cumulative totals are correlated with an R^2 of 0.248 ($p << 0.05$; Figure S5 in Supporting Information S1)—further suggesting inter-seasonal links that are driven by large-scale atmospheric processes, for example, wind-erosion intensities and dust transport patterns.

Temporal spread in the model products during the spring/summer pulse's onset period of February-March (Figure 7) begs the question of whether the onset date of the spring/summer pulse is shifting over time, even if absolute dust amounts are not. The timing and intensity of individual dust events are highly stochastic, however (Figure 4), and comparatively strong events (e.g., with maximum daily peaks exceeding one or even 2 μg/m^3) are not uncommon as early as January. Therefore, defining pulse onset by the earliest day that any absolute dust concentration threshold amount is exceeded is not well suited. Moving means can compensate somewhat for event-level stochasticity, but clear choices for moving window size and cumulative concentration thresholds are not readily apparent due to year-over-year variations. For consistency across and within years, we instead examine when a range of fractional annual cumulative dust thresholds are crossed, focusing on the ∼10%–25% thresholds that correspond to February through March (Figure 7b).

The onset date of the spring dust pulse, as measured by a range of threshold crossing dates, corresponds to a mean of February 28 for the 10% threshold and March 29/30 for the 25% threshold (Figure 8, Table 3). All thresholds examined exhibit similar trends over time and have similar uncertainties (1 s.d.) of 9–10 days. Threshold crossing dates exhibit insignificant or very weak correlations with several tested predictors including overall time (year), total annual dust, and total annual dust year-rank (Supplemental Table S1 and S2 in Supporting Information S1). Years that were strongly influenced by volcanic eruptions (1982/3 and 1992/3) were excluded from these regression analyses, but their inclusion or exclusion does not significantly affect the results described. In summary, these results suggest that there is little evidence that a) the onset timing of the spring pulse is shifting over time or b) earlier spring pulse onset dates are associated with dustier years.

Table 3
Summary of Crossing Dates for a Range of Fractional Cumulative Dust Thresholds Chosen to Screen for the Onset of the Spring/Summer Dust Pulse

Median day of year that cumulative dust thresholds were crossed				
Threshold	10%	15%	20%	25%
Day of Year ±1 s.d.	59.7 ± 9.83	72.6 ± 9.18	81.2 ± 9.74	89.7 ± 9.22
Calendar Date of Median	Feb 28	Mar 12/13	Mar 21/22	Mar 29/30

4.3. How Dusty Are the Dustiest Days? The Importance of Continuous Sampling

A small number of multi-day to multi-week dust events have outsized importance to atmospheric dust concentration patterns during any given year. To demonstrate the importance of these "dustiest" days, we sorted each day by its ranked dust abundance within each year to visualize the extent to which "X% of dust is present in Y days (or Y% of the days)" (Figure 9). Across all years examined, 50% of atmospheric surface dust is present in only 49–82 days of the year (13%–22% of the days). Phrased another way, the dustiest four weeks (7.7% of days) of each year contain between 20% and 35% of the annual dust at the site. For this study region near Hawaii, these dustiest days are almost always within the height of the spring/summer pulse in March through May (not shown).

The episodic character of dust transport, as demonstrated by the sequestration of large amounts of dust into relatively few days of the year, underscores an ongoing need for continuous sampling methodologies as a critical reference for intermittent sampling projects (e.g., oceanographic expeditions) and as a complement to diurnally restricted observations (e.g., at MLO through early 2011). Continuous sampling methods are more likely to capture the frequent but short-duration dust events that dominate atmospheric dust concentrations at remote oceanographic sites. Continuous records are also more likely to capture oceanographically significant fall and winter dust events that may be delivering (a) differentially sourced dust, if spring/summer and fall/winter pulses have different origins; and (b) differentially bioavailable dust, if fractional solubility and/or anthropogenic components of the bulk aerosols vary throughout the year. The extent of these different possibilities will be examined in forthcoming field data sets from the HATS project.

4.4. Dust Concentration and Precipitation Periodicity and Relationships With PDO

We focus on examining dust concentration variability in MERRA-2, but the atmospheric deposition of dust and its drivers, including precipitation and climatological forcing, are especially critical oceanographic factors.

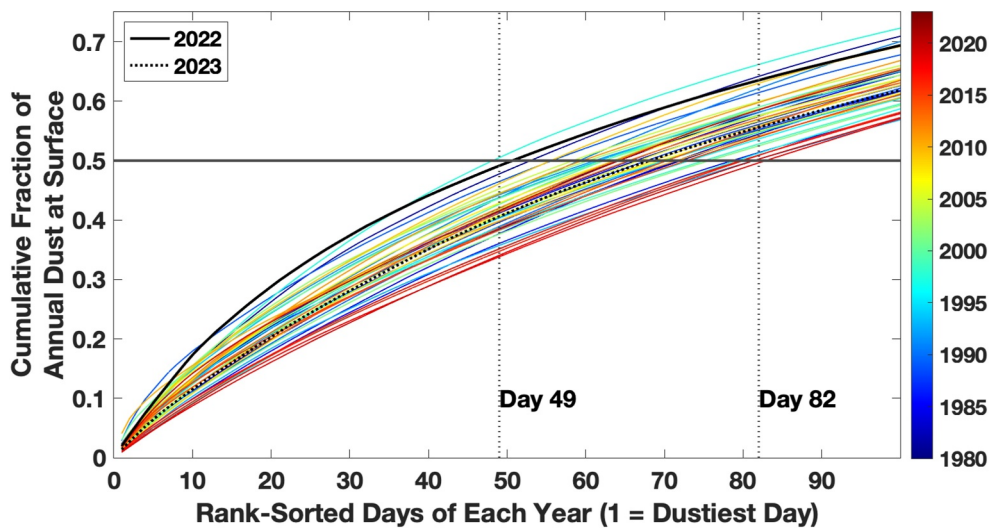

Figure 9. Cumulative fraction of annual surface dust (*y*-axis) as a function of rank-sorted "dustiest" days of each year (*x*-axis) for all years in the record (colors). The number of days required to account for 50% of the dust in the study domain is indicated by the intersection of the horizontal 50% line with the data. Minimum and maximum number of "dustiest" days required to account for half of total annual dust are indicated by vertical dotted lines and text annotations.

Precipitation is the primary driver, alongside scavenging (or washout), of wet deposition fluxes that typically dominate dust delivery in open ocean settings. Both dust transport and precipitation patterns have forcings that are linked to climatological indicators like the PDO index (Letelier, 2013), but these links are both spatially complex and non-linear. Dust flux by wet dust deposition, while reported by MERRA-2 on the same spatial scale as dust and precipitation, is even less well constrained and ground-truthed than the parameters we more cautiously examine here; though the extent of these uncertainties is the subject of considerable ongoing analysis.

Wavelet analyses of the MERRA-2 time-series—focusing on dust, narrow-field precipitation (as a higher-order link to wet dust deposition), and the previously invoked PDO index—suggests several interesting points. First, dust concentrations have consistent annual and semi-annual peaks in power, but little power at longer periods, at least within the time- and spatial domain examined. Coherence between dust concentrations and the PDO index is comparatively intermittent throughout the record, though occasionally this coherence is present on ∼1 year periodicity and is typically in-phase. Second, precipitation lacks a semi-annual period and is pre-dominantly annual in cycle, almost always preceding dust by ≈3-to-4 months (also evident in annual seasonality of the two shown in Figure S4 in Supporting Information S1). The mean lag between precipitation and dust (Figure 6e) may be decreasing over time, since around the year 2000 which also coincides with the onset of the Earth Observing System (Randles et al., 2017). Precipitation, even within the narrow spatial region examined here, has stronger multi-annual periodicity than does dust and thus exhibits stronger coherence with the PDO index. Coherence between precipitation and PDO is especially notable on 2- to 3-year timescales where the two variables appear predominantly anti-correlated with some evidence precipitation slightly precedes PDO.

Taken together, we encourage independent consideration of the two semi-annual dust pulses and their links to the upper ocean via both climatological parameters and wet deposition. Even neglecting the important potential for differences in fractional iron solubility and sourcing between the two pulses, the timing of the winter pulse—not the summer pulse—coincides with both the annual precipitation maximum and the ocean productivity maximum. This suggests the semi-annual winter dust pulse may have an outsized role in exerting oceanographic effects. Relatedly, the dominant spring/summer dust pulse and its rare but highly dusty days may obscure that pulse's connections to climatological forcings due to the very compressed timescale of its delivery. Differences between the two seasonal pulses, their links to wet and dry deposition, and their oceanographic consequences—including to ocean particle residence time—thus behoove more cautious and direct consideration.

We conducted a monthly binned linear correlation analysis for these time-series to examine the potential for different directionalities in relationships at different times of the year, but correlations between PDO, dust, and precipitation are significant in only a handful of months (not shown). We caution that our analysis is focused on a narrow ocean region, however. Precipitation rates (and thus, likely, wet dust deposition fluxes) are a) more spatially variable than dust concentrations are and b), based on the wavelet analysis, are more likely to respond to different components of atmospheric forcing and on different timescales (and lags) relative to PDO.

4.5. HATS Study Years: Specific Context for 2022 and 2023

The HATS project field years of 2022 and 2023 sampled the atmosphere and ocean for a wide range of elemental parameters using a combination of continuous (bulk atmospheric aerosol collections) and intermittent methods (rain events; marine particle profiles). To examine these specific years against the longer-term record, we calculated a daily Z-score for all datapoints by subtracting the 5-day mean-smoothed, day-of-year median trend and normalizing to the standard deviation of the complete data set. Time-series plots of daily Z-scores (Figure 10) are especially useful because moving averages of adjustable window length can identify both short- and long-term departures from the central tendency.

The 30-day (±15 days) moving mean Z-score (Figure 10; black line) tracks excursions of month-long significance that are especially relevant to seasonal oceanographic sampling campaigns like HATS. This metric indicates that 2022 was the dustiest year (and spring, specifically) in more than two decades—since 2001. The high magnitude of dust during spring 2022 is also evident when comparing the 2022 yearly ranking (7th dustiest of 44 in the record) and the spring/summer pulse's seasonal ranking (4th dustiest) to the rankings of the preceding two decades (Table S1 in Supporting Information S1). The Z-score dust metric reached a maximum of nearly +3 standard deviations on 10 April 2022, ending an otherwise unremarkable decade of dust concentrations that extends back to early 2013.

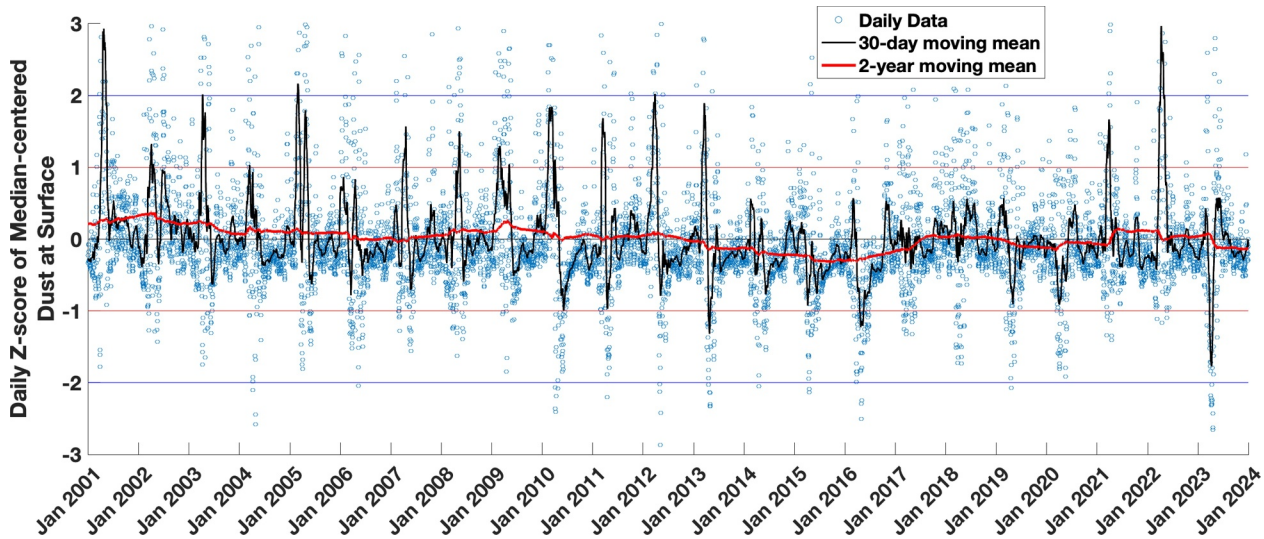

Figure 10. Time-series of daily dust Z-scores from 2001 through 2024. Moving mean trendlines with windows of 30 days (±15 days; black), and 2 years (±1 year; red) are shown. The strong positive excursion of the 30-day trend in April 2022 (far right) is the largest since 2001 (far left). A strong negative excursion or a dust "lull" in March-April 2023 is also anomalous compared to the preceding two decades, though less-intense negative excursions also below the −1 threshold occurred in 2010, 2013, and 2016.

By comparison, the 2023 calendar year (ranked 32 of 44 overall and similarly for both seasonal pulses) exhibited a notably strong "dust lull" or minimum during March and April. The extent of this lull is evident in Figure 11: it began in mid-March and reached a minimum of nearly 2 standard deviations below the central tendency on 9 April 2023. Dust concentrations returned to more typical levels by May. Similar though less intense spring dust lulls are present in the record in 2010, 2013, and 2016. Oceanographic sampling by HATS during the 2023 spring season coincided with this lull as well as the more typical late summer dust trends during May 2023 (cruise sampling dates shown as dots in Figure 11). Forthcoming field results from the HATS project will provide potentially strong contrasts between the very dusty spring of 2022 and the much less dusty 2023.

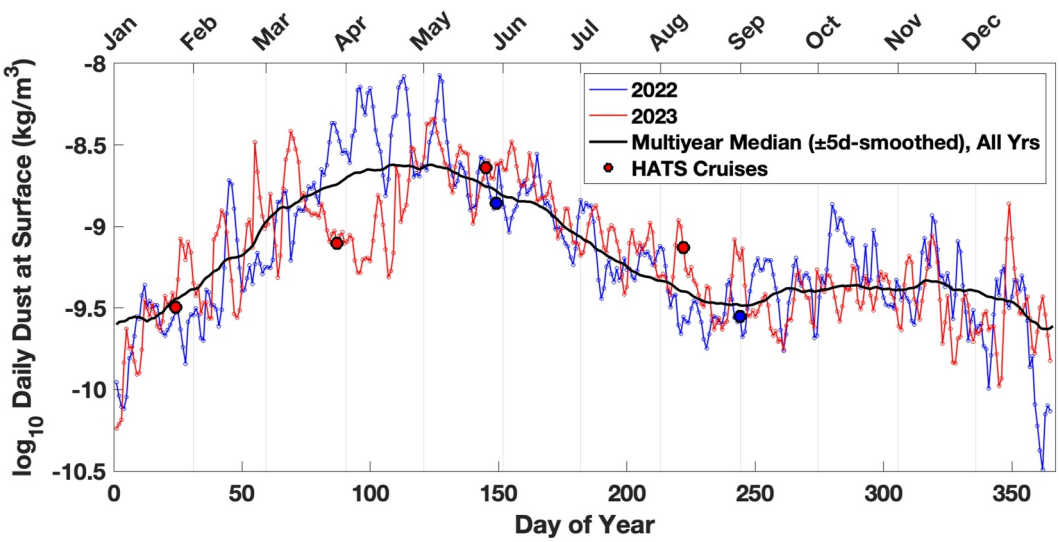

Figure 11. Dust concentrations in the study domain during the HATS sampling years of 2022 and 2023. HATS sampling cruises via the HOT program are indicated with color-coded dots, capturing the spring dust lull in late March 2023 and near-peak spring/summer dust in May 2022 and 2023. Land-based aerosol and precipitation collection occurred weekly throughout the 2-year sampling period.

5. Conclusions

This regional analysis of surface dust concentrations in the MERRA-2 reanalysis product describes the intensity, variability, timing, and long-term trends in dust transport to Hawaii and the surrounding ocean. Despite the stochastic nature of individual dust events, dust concentrations follow two broad seasonal pulses with fairly consistent timing and intensities on monthly to seasonal timescales. Total annual dust concentrations and the intensities of the seasonal dust pulses have not significantly changed over the more than four decades covered by the product, nor has the onset date of the dominant spring/summer dust pulse. Comparatively large amounts of dust are present during relatively few days of the year, underscoring the scientific value of continuous and near-continuous atmospheric monitoring efforts that are likely to capture major dust events and their potentially differential effects on ocean ecosystems in different seasons.

Time-series periodicity of dust shows clear power at annual and semi-annual scales, while precipitation in the ALOHA subdomain is predominantly annual. Precipitation at ALOHA more strongly coheres with the PDO index over multi-annual scales than does dust, suggesting precipitation and PDO may be linked via wet deposition, which coincides more with the winter dust pulse than the dominant spring/summer pulse. The power of PDO as a predictor of ecosystem limitation by either iron or macronutrients may thus be more subtly linked to the timing of dust delivery during productive fall/winter months by wet deposition than to bulk-increased atmospheric dust concentrations during the height of the spring dusty season. These relationships may be further complicated if the spring and winter dust pulses have differential sourcing, fractional solubility, or water column residence times.

Forthcoming field data from the HATS program will complement the high temporal and spatial coverage of the model reanalysis product examined here. Specifically, HATS participants and collaborators are measuring the multi-element composition of the seasonal dust pulses, their mineralogy and chemical lability; precipitation; and aerosol dust effects on marine particle composition and post-depositional chemical transformations. This atmospheric reanalysis extends our timescale of reference back to 1980 and shows that 2022 was an especially dusty year—the dustiest in over two decades—and that the spring of 2023 exhibited an anomalously low "lull" in dust during March and April. HATS sampling during these starkly contrasting years is likely to have captured important extremes in the strongly linked atmospheric and oceanic dust cycles.

Conflict of Interest

The authors declare no conflicts of interest relevant to this study.

Data Availability Statement

Primary data used to generate the results are publicly available through the Global Modeling Assimilation Office (GMAO, 2015). All code used to conduct the analyses and generate the figures are archived at Zenodo (Ohnemus, 2024).

Acknowledgments
This work was primarily supported by the National Science Foundation under Grant OCE-1949660 to CSB, DCO, and CMM. Additional support was provided by the University of Georgia via a COVID Impact Research Recovery Grant to DCO.

References

Anderson, R. F., Cheng, H., Edwards, R. L., Fleisher, M. Q., Hayes, C. T., Huang, K. F., et al. (2016). How well can we quantify dust deposition to the ocean? *Philosophical Transactions of the Royal Society A: Mathematical, Physical & Engineering Sciences*, *374*(2081), 20150285. https://doi.org/10.1098/rsta.2015.0285

Bates, N., Astor, Y., Church, M., Currie, K., Dore, J., Gonaález-Dávila, M., et al. (2014). A time-series view of changing ocean chemistry due to ocean uptake of anthropogenic CO2 and ocean acidification. *Oceanography*, *27*(1), 126–141. https://doi.org/10.5670/oceanog.2014.16

Black, E. E., Kienast, S. S., Lemaitre, N., Lam, P. J., Anderson, R. F., Planquette, H., et al. (2020). Ironing out Fe residence time in the dynamic upper ocean. *Global Biogeochemical Cycles*, *34*(9). https://doi.org/10.1029/2020gb006592

Black, E. E., Lam, P. J., Lee, J. M., & Buesseler, K. O. (2019). Insights from the 238U-234Th method into the coupling of biological export and the cycling of Cadmium, Cobalt, and manganese in the Southeast Pacific Ocean. *Global Biogeochemical Cycles*, *33*(1), 15–36. https://doi.org/10.1029/2018gb005985

Boyle, E. A., Bergquist, B. A., Kayser, R. A., & Mahowald, N. (2005). Iron, manganese, and lead at Hawaii Ocean Time-series station ALOHA: Temporal variability and an intermediate water hydrothermal plume. *Geochimica et Cosmochimica Acta*, *69*(4), 933–952. https://doi.org/10.1016/j.gca.2004.07.034

Bressac, M., Guieu, C., Doxaran, D., Bourrin, F., Desboeufs, K., Leblond, N., & Ridame, C. (2014). Quantification of the lithogenic carbon pump following a simulated dust-deposition event in large mesocosms. *Biogeosciences*, *11*(4), 1007–1020. https://doi.org/10.5194/bg-11-1007-2014

Bressac, M., Guieu, C., Ellwood, M. J., Tagliabue, A., Wagener, T., Laurenceau-Cornec, E. C., et al. (2019). Resupply of mesopelagic dissolved iron controlled by particulate iron composition. *Nature Geoscience*, *12*(12), 995–1000. https://doi.org/10.1038/s41561-019-0476-6

Browning, T. J., & Moore, C. M. (2023). Global analysis of ocean phytoplankton nutrient limitation reveals high prevalence of co-limitation. *Nature Communications*, *14*(1), 5014. https://doi.org/10.1038/s41467-023-40774-0

Buchard, V., Randles, C. A., da Silva, A. M., Darmenov, A., Colarco, P. R., Govindaraju, R., et al. (2017). The MERRA-2 aerosol reanalysis, 1980 onward. Part II: Evaluation and case studies. *Journal of Climate*, *30*(17), 6851–6872. https://doi.org/10.1175/jcli-d-16-0613.1

Buck, C. S., Aguilar-Islas, A., Marsay, C., Kadko, D., & Landing, W. M. (2019). Trace element concentrations, elemental ratios, and enrichment factors observed in aerosol samples collected during the US GEOTRACES eastern Pacific Ocean transect (GP16). *Chemical Geology*, *511*, 212–224. https://doi.org/10.1016/j.chemgeo.2019.01.002

Buck, C. S., Landing, W. M., & Resing, J. (2013). Pacific Ocean aerosols: Deposition and solubility of iron, aluminum, and other trace elements. *Marine Chemistry*, *157*, 117–130. https://doi.org/10.1016/j.marchem.2013.09.005

Conte, M. H., Carter, A. M., Koweek, D. A., Huang, S., & Weber, J. C. (2019). The elemental composition of the deep particle flux in the Sargasso Sea. *Chemical Geology*, *511*, 279–313. https://doi.org/10.1016/j.chemgeo.2018.11.001

Duce, R. A., & Tindale, N. W. (1991). Atmospheric transport of iron and its deposition in the ocean. *Limnology & Oceanography*, *36*(8), 1715–1726. https://doi.org/10.4319/lo.1991.36.8.1715

Fitzsimmons, J. N., Hayes, C. T., Al-Subiai, S. N., Zhang, R., Morton, P. L., Weisend, R. E., et al. (2015). Daily to decadal variability of size-fractionated iron and iron-binding ligands at the Hawaii Ocean Time-series Station ALOHA. *Geochimica et Cosmochimica Acta*, *171*, 303–324. https://doi.org/10.1016/j.gca.2015.08.012

Gelaro, R., McCarty, W., Suárez, M. J., Todling, R., Molod, A., Takacs, L., et al. (2017). The Modern-Era Retrospective analysis for research and Applications, version 2 (MERRA-2). *Journal of Climate*, *30*(Iss 13), 5419–5454. https://doi.org/10.1175/JCLI-D-16-0758.1

Global Modeling and Assimilation Office (GMAO) (2015). *tavg1_2d_aer_Nx: MERRA-2 2d,1-Hourly,Time-averaged,Single-Level,Assimilation, Aerosol diagnostics 0.625 x 0.5 degree, version 5.12.4*, : Goddard Space Flight Center Distributed Active Archive Center (GSFC DAAC), https://doi.org/10.5067/KLICLTZ8EM9D

Hamilton, D. S., Scanza, R. A., Rathod, S. D., Bond, T. C., Kok, J. F., Li, L., et al. (2020). Recent (1980 to 2015) trends and variability in daily-to-interannual soluble iron deposition from dust, fire, and anthropogenic sources. *Geophysical Research Letters*, *47*(17). https://doi.org/10.1029/2020gl089688

Hawco, N. J., Yang, S. C., Pinedo-González, P., Black, E. E., Kenyon, J., Ferrón, S., et al. (2022). Recycling of dissolved iron in the North Pacific subtropical gyre. *Limnology & Oceanography*, *67*(11), 2448–2465. https://doi.org/10.1002/lno.12212

Hayes, C. T., Fitzsimmons, J. N., Boyle, E. A., McGee, D., Anderson, R. F., Weisend, R., & Morton, P. L. (2015). Thorium isotopes tracing the iron cycle at the Hawaii Ocean Time-series Station ALOHA. *Geochimica et Cosmochimica Acta*, *169*, 1–16. https://doi.org/10.1016/j.gca.2015.07.019

Honjo, S. (1982). Seasonality and interaction of biogenic and lithogenic particulate flux at the Panama basin. *Science*, *218*(4575), 883–884. https://doi.org/10.1126/science.218.4575.883

Huang, S., & Conte, M. H. (2009). Source/process apportionment of major and trace elements in sinking particles in the Sargasso sea. *Geochimica et Cosmochimica Acta*, *73*(1), 65–90. https://doi.org/10.1016/j.gca.2008.08.023

Huneeus, N., Schulz, M., Balkanski, Y., Griesfeller, J., Prospero, J., Kinne, S., et al. (2011). Global dust model intercomparison in AeroCom phase I. *Atmospheric Chemistry and Physics*, *11*(15), 7781–7816. https://doi.org/10.5194/acp-11-7781-2011

Hyslop, N. P., Trzepla, K., Wallis, C. D., Matzoll, A. K., & White, W. H. (2013). Technical note: A 23-year record of twice-weekly aerosol composition measurements at Mauna Loa observatory. *Atmospheric Environment*, *80*, 259–263. https://doi.org/10.1016/j.atmosenv.2013.07.038

Jickells, T., & Moore, C. M. (2015). The importance of atmospheric deposition for ocean productivity. *Annual Review of Ecology, Evolution and Systematics*, *46*(1), 481–501. https://doi.org/10.1146/annurev-ecolsys-112414-054118

Jickells, T. D., Baker, A. R., & Chance, R. (2016). Atmospheric transport of trace elements and nutrients to the oceans. *Philos Trans A Math Phys Eng Sci*, *374*(2081), 20150286. https://doi.org/10.1098/rsta.2015.0286

Kadko, D., Landing, W. M., & Buck, C. S. (2020). Quantifying atmospheric trace element deposition over the ocean on a global scale with satellite rainfall products. *Geophysical Research Letters*, *47*(7). https://doi.org/10.1029/2019gl086357

Kadko, D., Landing, W. M., & Shelley, R. U. (2015). A novel tracer technique to quantify the atmospheric flux of trace elements to remote ocean regions. *Journal of Geophysical Research: Oceans*, *120*(2), 848–858. https://doi.org/10.1002/2014jc010314

Karl, D. M., Christian, J. R., Dore, J. E., Hebel, D. V., Letelier, R. M., Tupas, L. M., & Winn, C. D. (1996). Seasonal and interannual variability in primary production and particle flux at Station ALOHA. *Deep Sea Research Part II: Topical Studies in Oceanography*, *43*(2–3), 539–568. https://doi.org/10.1016/0967-0645(96)00002-1

Karl, D. M., & Lukas, R. (1996). The Hawaii Ocean Time-series (HOT) program: Background, rationale and field implementation. *Deep Sea Research Part II: Topical Studies in Oceanography*, *43*(2–3), 129–156. https://doi.org/10.1016/0967-0645(96)00005-7

Kok, J. F., Adebiyi, A. A., Albani, S., Balkanski, Y., Checa-Garcia, R., Chin, M., et al. (2021). Contribution of the world's main dust source regions to the global cycle of desert dust. *Atmospheric Chemistry and Physics*, *21*(10), 8169–8193. https://doi.org/10.5194/acp-21-8169-2021

Lamborg, C. H., Buesseler, K. O., Valdes, J., Bertrand, C. H., Bidigare, R., Manganini, S., et al. (2008). The flux of bio- and lithogenic material associated with sinking particles in the mesopelagic "twilight zone" of the northwest and North Central Pacific Ocean. *Deep Sea Research Part II: Topical Studies in Oceanography*, *55*(14–15), 1540–1563. https://doi.org/10.1016/j.dsr2.2008.04.011

Letelier, R. M., Bjorkman, K. M., Church, M. J., Hamilton, D. S., Mahowald, N. M., Scanza, R. A., et al. (2019). Climate-driven oscillation of phosphorus and iron limitation in the North Pacific subtropical gyre. *Proceedings of the National Academy of Sciences of the United States of America*, *116*(26), 12720–12728. https://doi.org/10.1073/pnas.1900789116

Mahowald, N. M., Baker, A. R., Bergametti, G., Brooks, N., Duce, R. A., Jickells, T. D., et al. (2005). Atmospheric global dust cycle and iron inputs to the ocean. *Global Biogeochemical Cycles*, *19*(4). https://doi.org/10.1029/2004gb002402

Marsay, C. M., Kadko, D., Landing, W. M., & Buck, C. S. (2022). Bulk aerosol trace element concentrations and deposition fluxes during the U.S. GEOTRACES GP15 Pacific meridional transect. *Global Biogeochemical Cycles*, *36*(2). https://doi.org/10.1029/2021gb007122

Mathworks MATLAB version: R2023b (2023). The MathWorks inc., Natick, Massachusetts, United States. Retrieved from https://www.mathworks.com

Ohnemus, D. C. (2024). capecodnative/HawaiiDust: Initial release (Version v1.0). *Zenodo*. https://doi.org/10.5281/ZENODO.14207482

Ohnemus, D. C., & Lam, P. J. (2015). Cycling of lithogenic marine particles in the US GEOTRACES North Atlantic transect. *Deep Sea Research Part II: Topical Studies in Oceanography*, *116*, 283–302. https://doi.org/10.1016/j.dsr2.2014.11.019

Randles, C. A., da Silva, A. M., Buchard, V., Colarco, P. R., Darmenov, A., Govindaraju, R., et al. (2017). The MERRA-2 aerosol reanalysis, 1980 - Onward, Part I: System description and data assimilation evaluation. *Journal of Climate*, *30*(17), 6823–6850. https://doi.org/10.1175/JCLI-D-16-0609.1

Rijkenberg, M. J. A., Gerringa, L. J. A., Timmermans, K. R., Fischer, A. C., Kroon, K. J., Buma, A. G. J., et al. (2008). Enhancement of the reactive iron pool by marine diatoms. *Marine Chemistry*, *109*(1–2), 29–44. https://doi.org/10.1016/j.marchem.2007.12.001

Pacific Decadal Oscillation (PDO) based on ERSST-5 (2024). National Oceanic and Atmospheric Administration. *National Centers for Environmental Information (NOAA NCEI)*. Retrieved from https://www.ncei.noaa.gov/access/monitoring/pdo/

Schroth, A. W., Crusius, J., Sholkovitz, E. R., & Bostick, B. C. (2009). Iron solubility driven by speciation in dust sources to the ocean. *Nature Geoscience*, *2*(5), 337–340. https://doi.org/10.1038/ngeo501

Schulz, M., Prospero, J. M., Baker, A. R., Dentener, F., Ickes, L., Liss, P. S., et al. (2012). Atmospheric transport and deposition of mineral dust to the ocean: Implications for research needs. *Environmental Science and Technology*, *46*(19), 10390–10404. https://doi.org/10.1021/es300073u

Tagliabue, A., Buck, K. N., Sofen, L. E., Twining, B. S., Aumont, O., Boyd, P. W., et al. (2023). Authigenic mineral phases as a driver of the upper-ocean iron cycle. *Nature*, *620*(7972), 104–109. https://doi.org/10.1038/s41586-023-06210-5

Weis, J., Schallenberg, C., Chase, Z., Bowie, A. R., Wojtasiewicz, B., Perron, M. M. G., et al. (2022). Southern Ocean phytoplankton stimulated by wildfire emissions and sustained by iron recycling. *Geophysical Research Letters*, *49*(11). https://doi.org/10.1029/2021gl097538

Winton, V. H. L., Dunbar, G. B., Bertler, N. A. N., Millet, M. A., Delmonte, B., Atkins, C. B., et al. (2014). The contribution of aeolian sand and dust to iron fertilization of phytoplankton blooms in southwestern Ross Sea, Antarctica. *Global Biogeochemical Cycles*, *28*(4), 423–436. https://doi.org/10.1002/2013gb004574

Wu, M., Liu, X., Yu, H., Wang, H., Shi, Y., Yang, K., et al. (2020). Understanding processes that control dust spatial distributions with global climate models and satellite observations. *Atmospheric Chemistry and Physics*, *20*(22), 13835–13855. https://doi.org/10.5194/acp-20-13835-2020

Erratum

The originally published version of this article contained an error in the author contributions. Coauthor Mariah Ricci should be credited with the following contributions: investigation, writing – original draft, and writing – review & editing. The error has been corrected, and this may be considered the authoritative version of record.